

Ultrafast Spatiotemporal Dynamics of Terahertz Generation by Ionizing Two-Color Femtosecond Pulses in Gases

I. Babushkin,¹ W. Kuehn,² C. Köhler,³ S. Skupin,^{3,4} L. Bergé,⁵ K. Reimann,² M. Woerner,² J. Herrmann,² and T. Elsaesser²

¹Weierstraß-Institut für Angewandte Analysis und Stochastik, 10117 Berlin, Germany

²Max-Born-Institut für Nichtlineare Optik und Kurzzeitspektroskopie, 12489 Berlin, Germany

³Max Planck Institute for the Physics of Complex Systems, 01187 Dresden, Germany

⁴Friedrich Schiller University, Institute of Condensed Matter Theory and Optics, 07743 Jena, Germany

⁵CEA-DAM, DIF, 91297 Arpajon, France

(Received 9 March 2010; published 28 July 2010)

We present a combined theoretical and experimental study of spatiotemporal propagation effects in terahertz (THz) generation in gases using two-color ionizing laser pulses. The observed strong broadening of the THz spectra with increasing gas pressure reveals the prominent role of spatiotemporal reshaping and of a plasma-induced blueshift of the pump pulses in the generation process. Results obtained from (3 + 1)-dimensional simulations are in good agreement with experimental findings and clarify the mechanisms responsible for THz emission.

DOI: [10.1103/PhysRevLett.105.053903](https://doi.org/10.1103/PhysRevLett.105.053903)

PACS numbers: 42.65.Re, 32.80.Fb, 52.50.Jm

Far-infrared radiation in the THz range has developed into a sensitive probe of low-frequency excitations of condensed matter and into an analytical and imaging tool for a broad range of applications. Recently, intense THz pulses have been applied for inducing nonlinear light-matter interactions and for studying quantum-coherent charge transport phenomena in solids. In this new area of research, the generation of well-defined THz field transients with a high amplitude represents a key issue. Both electron accelerator- and laser-based sources have been developed to generate THz transients. Conventional laser-driven THz sources are based on semiconductor photoconductive switches [1] and nonlinear frequency conversion in crystals [2–5], providing a comparably small THz field strength in a spectral range limited by the absorption of the crystals. In an alternative approach [6], a short pump pulse at 800 nm and its second harmonic at 400 nm are focused into a gas to generate a plasma. Intense THz pulses with field amplitudes as high as 400 kV/cm and remarkably broad spectra have been reported with this method [5–14]. However, the physical mechanisms behind the observed THz generation remain controversial. Initially, THz generation has been explained by four-wave mixing rectification via Kerr nonlinearity [6] or, more recently, ponderomotive and relativistic effects in the plasma [15], and experimental results have been interpreted along those lines (see, e.g., [7–11]). In contrast, other studies attribute THz emission to a laser-induced plasma current in the asymmetric two-color laser field [12,13,16]. So far, theoretical work has mainly focused on the analysis of local fields by using photocurrent models. An alternative approach is based on particle in cell simulations [17] which are computationally very expensive and limited to propagation lengths of only a few micrometers.

In this Letter we present a combined theoretical and experimental study of THz generation by ionizing two-color femtosecond pulses in a gas. Extensive numerical simulations were performed using for the first time a (3 + 1)-dimensional code based on a unidirectional pulse propagation equation, which includes the plasma dynamics responsible for THz generation. This approach allows a comprehensive description of the propagation of all fields taking into account their spatio-temporal reshaping induced by the plasma effects and by the optical Kerr nonlinearity. We demonstrate that spatio-temporal propagation effects are indispensable for understanding the generation process and influence the THz spectrum substantially. In both experiment and simulation we observe a remarkable broadening of the THz spectrum with increasing gas pressure. Such broadening is a result of a sensitive dependence of the THz spectrum on small phase and frequency shifts induced by nonlinear propagation of the fundamental and second-harmonic pulses. We show that the stepwise character of the ionization process on the subfemtosecond time scale is essential for such dependence.

Our THz plasma source (inset of Fig. 1) is driven by 40 fs pulses (800 nm) with pulse energies of $\sim 300 \mu\text{J}$ at a repetition rate of 1 kHz from a Ti:sapphire laser system. Intensities far above the field ionization threshold are reached by focusing the beam of 8 mm diameter with an achromatic lens (L) of 40 mm focal length. A 0.1 mm thin β -barium borate (BBO) crystal (C) cut for type I second-harmonic generation is additionally inserted into the convergent beam 7 mm before the focus. The setup is placed in a closed chamber filled with argon at various pressures between 1 and 1000 mbar. THz radiation emitted from the plasma volume in the focal spot is collected by a parabolic mirror (M) with a diameter of 25.4 mm at a distance of its

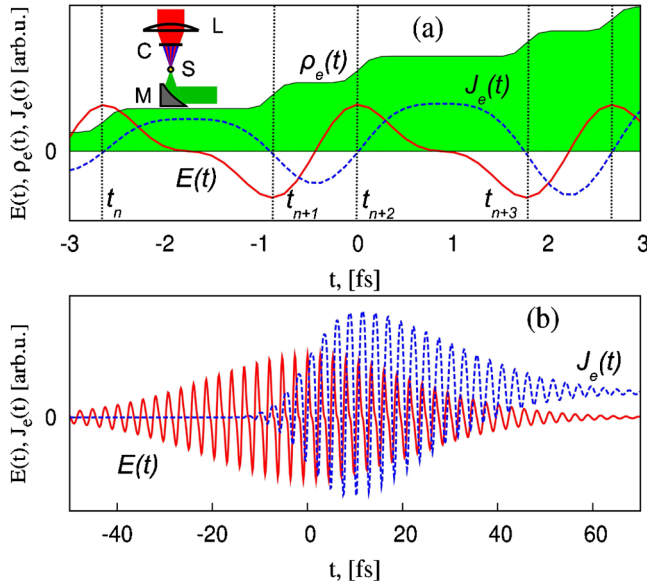


FIG. 1 (color online). The mechanism of THz generation: (a) The two-color electric field E generates free electrons with a stepwise modulation of the electron density ρ_e via tunneling photoionization. The ionization occurs mostly near the maxima of electric field at time instances t_n . This leads to a slow component of the current J_e (b) which acts as a source for THz emission. Inset in (a): scheme of the experimental setup.

focal length of 12.7 mm. Intensity interferograms were recorded with a mercury cadmium telluride (HgCdTe) detector by varying the path difference between the two arms of a Michelson interferometer. THz spectra were derived by Fourier transformation.

For the description of the nonlinear propagation of electromagnetic fields valid in the full range from THz down to UV or VUV wavelengths beyond paraxial and slowly varying envelope approximations, we use the following unidirectional pulse propagation equation [18] for linearly polarized pulses,

$$\partial_z \hat{E} = i\sqrt{k(\omega)^2 - k_x^2 - k_y^2} \hat{E} + i\frac{\mu_0 \omega^2}{2k(\omega)} \hat{P}_{\text{NL}}. \quad (1)$$

Here, $\hat{E}(k_x, k_y, z, \omega)$ is the Fourier transform (indicated by $\hat{}$) of the electric field with respect to x , y , and t , $k(\omega) = \omega n(\omega)/c$ is the wave number, $\nu = \omega/2\pi$ the frequency, c is the speed of light and $n(\omega)$ is the refractive index of the gas, in our case argon [19]. The first term on the right-hand side of Eq. (1) describes linear dispersion and diffraction of the pulse. The nonlinear polarization $\hat{P}_{\text{NL}} = \hat{P}_{\text{Kerr}} + i\hat{J}_e/\omega + i\hat{J}_{\text{loss}}/\omega$ originates from the optical Kerr effect P_{Kerr} , the electron current J_e and a loss term J_{loss} due to photon absorption during ionization. In Eq. (1), radiation in backward direction is neglected, as it does neither influence the propagation of the forward fields, nor is it detected in our experiment. In \hat{P}_{Kerr} we take into account different nonlinear susceptibilities for neutral atoms and ions [20]. The plasma dynamics is described by the electron density $\rho_e(t)$, obeying $\dot{\rho}_e(t) = W_{\text{ST}}(E)[\rho_{\text{at}} - \rho_e(t)]$, where ρ_{at} de-

notes the neutral atomic density and dot the time-derivative. We use the quasistatic tunneling ionization rate for hydrogenlike atoms given by [13] $W_{\text{ST}}(E) = 4\omega_a(r_H)^{2.5}[E_a/|E|]\exp[-2(r_H)^{1.5}E_a/3|E|]$, where $E_a = m_e^2 q^5 / (4\pi\epsilon_0)^3 \hbar^4$, $\omega_a = m_e q^4 / (4\pi\epsilon_0)^2 \hbar^3$, and $r_H = U_{\text{Ar}}/U_h$. U_h and U_{Ar} are the ionization potentials of hydrogen and argon; m_e and q are the electron mass and charge, respectively. For the anticipated electric field strengths, we neglect multiphoton and avalanche ionization. The transverse macroscopic plasma current $J_e(t)$ is determined by the microscopic velocity distribution $v(t, t_0)$ of electrons born at the time t_0 [12,13],

$$J_e(t) = q \int_{-\infty}^t v(t, t_0) \dot{\rho}_e(t_0) dt_0. \quad (2)$$

Assuming zero velocity for new-born electrons and neglecting the influence of the magnetic field and electron-electron interaction, the electron velocity reads $v(t, t_0) = \frac{q}{m_e} \int_{t_0}^t E(\tau) \exp[-\nu_e(t-\tau)] d\tau$, where ν_e is the electron-ion collision rate. Substituting this into Eq. (2) we obtain

$$\dot{J}_e(t) + \nu_e J_e(t) = \frac{q^2}{m_e} E(t) \rho_e(t). \quad (3)$$

The above analysis demonstrates that we regain a well-known equation for the current (see, e.g., [20]). To formally ensure energy conservation during ionization, the additional term $J_{\text{loss}} = W_{\text{ST}}(E)(\rho_{\text{at}} - \rho_e)U_{\text{Ar}}/E$ is introduced in Eq. (1) accounting for ionization energy loss.

Let us now illustrate the mechanism behind THz generation. In Fig. 1(a) we present the electron density, which shows a stepwise increase near the tunnel ionization events at the field maxima. Such behavior has been recently observed in real-time experiments with subfemtosecond resolution [21]. In a simplified model, we can assume rectangular steps in the electron density [$\dot{\rho}_e(t) = \sum_n \rho_n \delta(t - t_n)$] and $\nu_e = 0$, and thereby obtain a discrete version of Eq. (2)

$$J_e(t) \sim \sum_n \rho_n H(t - t_n) [v_f(t) - v_f(t_n)], \quad (4)$$

where $H(t)$ is the Heaviside step function, $v_f(t) = \frac{q}{m_e} \int_{-\infty}^t E(\tau) d\tau$ is the free electron velocity such that $v(t, t_n) = [v_f(t) - v_f(t_n)]$, and ρ_n is the electron density created in the n th ionization event. For a monochromatic electric field $v_f(t_n) = 0$. Here, the Fourier transform of the term $H(t - t_n)v_f(t_n)$ exhibits a low-frequency spectrum $\propto 1/\omega$. Therefore, THz radiation is generated by the second term in Eq. (4) proportional to $v_f(t_n)$, while the first term contributes in the spectral range of the pump fields. We checked that four-wave mixing rectification by Kerr effect or ponderomotive plasma effects [15] provides a THz yield more than three orders of magnitudes smaller than the ionization current [Eq. (4)].

To model the experimental conditions in the plasma spot, we consider a Gaussian input beam with a waist $w_0 = 100 \mu\text{m}$ and a duration of the 800 nm pump pulse of (FWHM) $t_p = 40$ fs (pulse energy 300 μJ). The inten-

sity of the second harmonic at 400 nm is chosen as 12% of the fundamental as estimated from the experiment. The duration t_p and the waist w_0 of the second harmonic are smaller than the values for the fundamental by a factor $\sqrt{2}$. The phase angle between the two components is initially zero and shifts during propagation to nonzero values. The pulsed input beams are focused ($f = 0.5$ mm, to have a comparable ratio w_0/f in experiment and simulation) into the argon atmosphere. Figure 2 shows (a) the evolution of the computed plasma density and the transverse distribution of the THz field at (b) 0.2 mm and (c) 1 mm for a gas pressure of 200 mbar. The field intensities reach the ionization threshold shortly after the starting point of the simulation at $z = 0$ mm, and form a 0.7 mm long plasma channel. THz fields inside this focal region reach values of the order of GV/m and exhibit a strong diffraction.

Let us now investigate the dependence of THz generation on the gas pressure. Measured spectra over the complete pressure range between 1 and 1000 mbar are shown as a contour plot in Fig. 3(a). Our HgCdTe detector is sensitive in a frequency range from 20 to 170 THz. For a comparison of theory and experiment, this high-frequency part of the spectra is most relevant. Figure 3(c) shows a low-frequency spectrum with the characteristic maximum below 5 THz, in agreement with the simulated spectra.

In our setup, we mainly detect THz radiation generated in the focus of the mirror (M). Simple ray tracing estimates indicate that the length of this focal region is ≈ 0.3 mm. The almost vanishing spectrum at small argon pressure clearly shows that the plasma and not the BBO crystal acts as a source of the emitted radiation. In the region from zero to ~ 300 mbar the spectral width increases strongly. The highest frequencies even beyond 50 THz are detected at pressures larger than 300 mbar. Above ~ 500 mbar the slope of the high-frequency wing stays rather constant. The measured THz yield [solid line in Fig. 3(e)] grows linearly with pressure up to 400 mbar before it saturates.

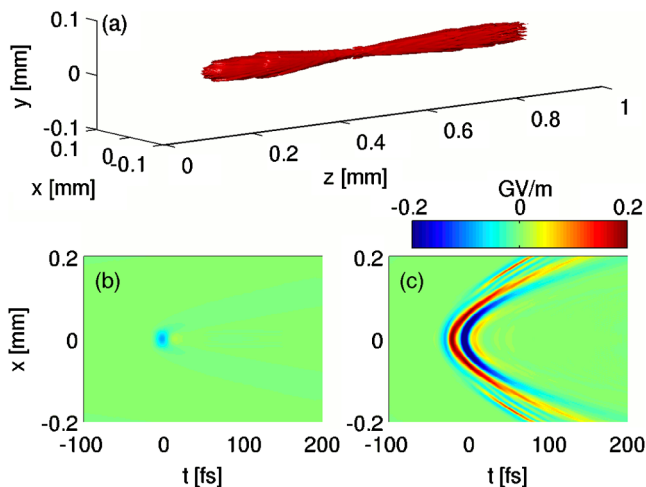


FIG. 2 (color online). (a) Iso-electron-density surface at $\rho_e = 5 \times 10^{17} \text{ cm}^{-3}$ for 200 mbar gas pressure. Computed THz fields ($\nu < 80$ THz) at (b) $z = 0.2$ mm and at (c) $z = 1$ mm.

In Figs. 3(b) and 3(d), THz spectra computed with our simulation code are shown. These spectra are obtained by integration over the transverse coordinates (x, y). We find very good agreement between experiment and simulation below 500 mbar for THz fields generated at the beginning of the plasma spot around $z = 0.2$ mm (0.3 mm before the linear focus). THz fields generated upon further propagation become spectrally much broader. Hence, we conjecture that the parabolic mirror in the experiment images the leading part of the plasma spot only. The calculated THz yield increases linearly with gas pressure [dashed line in Fig. 3(e)], in agreement with experimental results up to 400 mbar. The saturation of the experimental yield at higher pressure is likely due to additional THz losses upon further propagation towards the mirror, whereas the simulated yield is computed directly at the position $z = 0.2$ mm.

The observed pressure dependence of the THz spectral maximum and width gives insight into important features of plasma-induced THz generation. The dependence of the spectral width on pressure can not be explained by the local plasma current, in which the variation of pressure only results in an amplitude scaling of the current. Instead, it originates from pressure dependent nonlinear propagation effects. For the intensity range and plasma interaction length of the experiment, the calculated spectral evolution of the pump pulses at 400 nm ($\nu = 750$ THz) and 800 nm ($\nu = 375$ THz) shows that their spectral broadening is negligible. We observe, however, small blue-shifts $\delta\nu$ of the central frequencies caused by the nonlinear plasma-induced change of the refractive index [22,23]. These shifts are ~ 1 THz in the fundamental and ~ 0.4 THz in

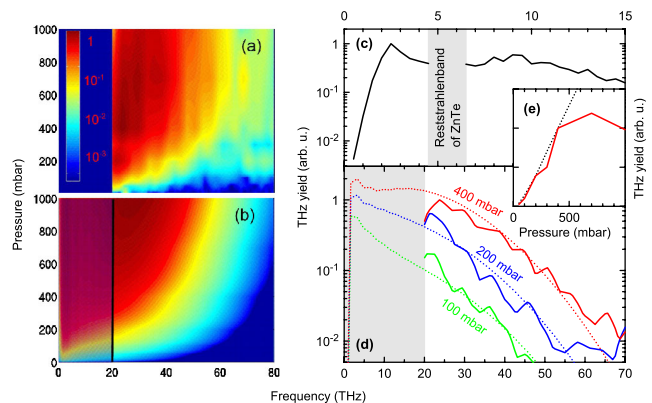


FIG. 3 (color online). Measured THz spectra (a) and simulation results (b) for pressures between 1 and 1000 mbar. In (d), experimental (solid lines) and theoretical (dashed lines) spectra are compared for various pressures. In (e), the overall THz yield versus pressure is shown (simulation: dashed line, experiment: solid line). (c) Low-frequency spectrum for 1000 mbar measured by electro-optic sampling in ZnTe, corrected for the frequency-dependent detector response [24]. Shading signifies frequency ranges where no experimental data are available.

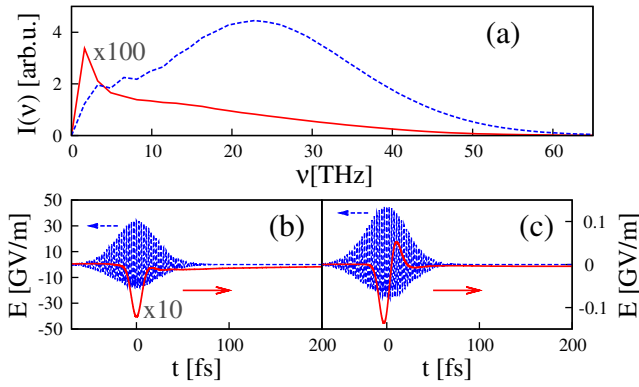


FIG. 4 (color online). (a) On-axis ($x = 0$, $y = 0$) spectral intensity $I(\nu)$ at $z = 0.1$ mm (solid line) and at $z = 0.2$ mm (dashed line). (b, c) Temporal shape of $E(t)$ (dashed line) and of its low-frequency part (solid line) for 400 mbar gas pressure at (b) $z = 0.1$ mm and at (c) $z = 0.2$ mm. In (a) and (b), $I(\nu)$ and $E(t)$ at $z = 0.1$ mm are amplified by factors of 100 and 10, respectively, to improve visibility.

the second harmonic at $z = 0.2$ mm for 400 mbar, and depend strongly on the gas pressure.

Surprisingly, these very small frequency shifts have a dramatic influence on the generated THz spectrum. This effect is most pronounced in the on-axis spectra, where the intensity is maximal. In Fig. 4(a), the calculated on-axis THz spectra are plotted for 400 mbar gas pressure, displaying between 0.1 and 0.2 mm dramatic changes in spectral shape and in the maximum frequency. Figures 4(b) and 4(c) show the corresponding time-dependent field and its low-frequency part. To explain the physical origin of this very sensitive dependence, let us go back to our simplified model [Eq. (4)]. For a two-color optical field, $E = A_1 \cos[(\omega_0 + \delta\omega)t] + A_2 \cos(2\omega_0 t + \theta)$, the field maxima in every half-cycle are given by $\omega_0 t_n \approx n\pi - n\pi\delta\omega/\omega_0 - (-1)^n 2r \sin\theta$, provided that $A_2/A_1 = r \ll 1$ and $n\delta\omega \ll \omega_0$. Hence, t_n and therefore the free electron velocities $v_f(t_n)$ can alter significantly when $\delta\omega$ (and θ) change upon the propagation. As seen above, the low-frequency spectrum is determined by a sum over contributions $\sim v_f(t_n)$, and this sum finally determines the THz spectral shape in Fig. 4(a). In the full (3 + 1)-dimensional geometry, the spectral shapes generated at different spatial points are added and averaged, leading to the strong spectral broadening observed in Fig. 3(d). Thus, the dependence of the THz spectra on pressure and propagation distance are explained by propagation effects of the pump fields. We would like to stress that phase and frequency relation of fundamental and second-harmonic fields change during propagation.

In conclusion, we presented a theoretical and experimental investigation of photocurrent induced THz gen-

eration. Using (3 + 1)-dimensional simulations and experimental measurements we show a strong dependence of the THz spectra on gas pressure. Our results give insight into the important influence of nonlinear propagation effects and the mechanism of THz generation. Plasma-induced blueshifts of the driving pulses play a key role in the broadening of the THz spectra and confirm that the THz emission process is associated with a stepwise modulation of the tunneling ionization current. We believe that our findings open interesting perspectives to control THz emission in a broader spectral range.

This work has been performed using HPC resources from GENCI-CINES (Grant 2009-x2009106003). I. B. gratefully acknowledges financial support by DFG.

- [1] D. You, R. R. Jones, P. H. Bucksbaum, and D. R. Dykaar, *Opt. Lett.* **18**, 290 (1993).
- [2] D. H. Auston, K. P. Cheung, J. A. Valdmanis, and D. A. Kleinman, *Phys. Rev. Lett.* **53**, 1555 (1984).
- [3] K.-L. Yeh *et al.*, *Appl. Phys. Lett.* **90**, 171121 (2007).
- [4] A. G. Stepanov *et al.*, *Opt. Lett.* **33**, 2497 (2008).
- [5] K. Reimann, *Rep. Prog. Phys.* **70**, 1597 (2007).
- [6] D. J. Cook and R. M. Hochstrasser, *Opt. Lett.* **25**, 1210 (2000).
- [7] J. Dai *et al.*, *Phys. Rev. Lett.* **97**, 103903 (2006).
- [8] M. Kress, T. Loeffler, S. Eden, M. Thomson, and H. G. Roskos, *Opt. Lett.* **29**, 1120 (2004).
- [9] T. Bartel *et al.*, *Opt. Lett.* **30**, 2805 (2005).
- [10] Xu Xie, J. Dai, and X.-C. Zhang, *Phys. Rev. Lett.* **96**, 075005 (2006).
- [11] A. Houard, Yi Liu, B. Prade, and A. Mysyrowicz, *Opt. Lett.* **33**, 1195 (2008).
- [12] K. Kim, J. Glowina, A. Taylor, and G. Rodriguez, *Opt. Express* **15**, 4577 (2007); *Nat. Photon.* **2**, 605 (2008).
- [13] M. D. Thomson, M. Kress, T. Loeffler, and H. G. Roskos, *Laser Photon. Rev.* **1**, 349 (2007).
- [14] M. Kress *et al.*, *Nature Phys.* **2**, 327 (2006).
- [15] J. Peñano *et al.*, *Phys. Rev. E* **81**, 026407 (2010).
- [16] K. Kim, *Phys. Plasmas* **16**, 056706 (2009).
- [17] H.-Ch. Wu, J. Meyer-ter-Vehn, and Zh.-M. Sheng, *New J. Phys.* **10**, 043001 (2008); M. Chen, A. Pukhov, X.-Yu Peng, and O. Willi, *Phys. Rev. E* **78**, 046406 (2008); W.-M. Wang *et al.*, *Opt. Express* **16**, 16999 (2008).
- [18] M. Kolesik and J. V. Moloney, *Phys. Rev. E* **70**, 036604 (2004).
- [19] A. Dalgarno and A. E. Kingston, *Proc. R. Soc. A* **259**, 424 (1960).
- [20] P. Sprangle, J. R. Peñano, B. Hafizi, and C. A. Kapetanios, *Phys. Rev. E* **69**, 066415 (2004).
- [21] M. Uiberacker *et al.*, *Nature (London)* **446**, 627 (2007).
- [22] W. M. Wood, C. W. Siders, and M. C. Downer, *Phys. Rev. Lett.* **67**, 3523 (1991).
- [23] S. C. Rae and K. Burnett, *Phys. Rev. A* **46**, 1084 (1992).
- [24] A. Leitenstorfer *et al.*, *Appl. Phys. Lett.* **74**, 1516 (1999).